

Electrodifusional Wall Shear Rate Analysis in Scraped Surface Heat Exchanger

Eric Dumont

Dépt. Génie des Procédés Alimentaires, Ecole Nationale Supérieure d'Ingénieurs des Techniques Agricoles et Alimentaires, 44322 Nantes Cedex 3, France

Laboratoire de Génie des Procédés-UPRES EA 1152, Université de Nantes, 44602 Saint Nazaire Cedex, France

Francine Fayolle

Dépt. Génie des Procédés Alimentaires, Ecole Nationale Supérieure d'Ingénieurs des Techniques Agricoles et Alimentaires, 44322 Nantes Cedex 3, France

Jack Legrand

Laboratoire de Génie des Procédés—UPRES EA 1152, Université de Nantes, 44602 Saint Nazaire Cedex, France

An electrochemical technique was used to measure local and instantaneous wall shear rates in a scraped surface heat exchanger (SSHE). The inner cylinder, equipped with two blades symmetrically opposed, was driven by a stepping motor and the outer cylinder was fixed. Highly viscous Newtonian fluids (Emkarox HV45 solutions) and non-Newtonian model fluids (aqueous solutions of guar and CMC) were used. The reliability of the electrochemical technique was validated for these fluids in an annular space (SSHE without blades). The evolution of the limiting diffusion current was given by the probes in a scraping situation. In the general case of scraping, the flow was unsteady, and very fast large fluctuations of the limiting diffusion current were measured. The shear rate at the wall of the stator of the SSHE appeared fully controlled by the rotation of the blades. Then, electrodiffusion measurements were interpreted using three different wall shear rate calculating procedures. Wall shear rate in SSHE appeared ten to 100 times more important than in annulus, and the lowest values of the clearance between the edge of the blades and the stator was about 50×10^{-6} m.

Introduction

Electrodifusion probes mounted flush to a wall are largely used to measure the wall shear rate in order to study various hydrodynamic problems (Hanratty, 1991). Thus, the well-known Taylor-Couette flow is often studied using circular probes (Kataoka et al., 1977; Legrand et al., 1983; Wronski and Jastrzebski, 1990) or three-segment probes (Sobolík et al., 1995), and the results obtained show more clearly the nature of the transition between laminar flow and fully developed turbulent flow. These studies are of particular interest, because a great number of industrial applications are based on the flow between two concentric cylinders, such as scraped surface heat exchangers.

Scraped surface heat exchangers (SSHE), mainly used in the food industry, allow the processing of highly viscous fluids with complex rheology (cream cheese, fruit concentrate, ice cream, among others). The specificity of these exchangers lies in the rotation of a shaft equipped with blades that periodically scrape the exchange surface in order to prevent crust formation and to promote heat transfer (Figure 1). In this type of exchanger, the flow pattern is the result of the superposition of a Poiseuille flow in an annular space and a Couette flow, to which perturbations created by the blades are added. This flow pattern is particularly complex, and has only been superficially studied directly (Trommelen and Beek, 1971a; Naimi, 1989; Burmester et al., 1996). Most of the works on the subject tend to model the geometry of the SSHE as an annular space without blades (Härröd, 1986; Abichandani et

Correspondence concerning this article should be addressed to J. Legrand.

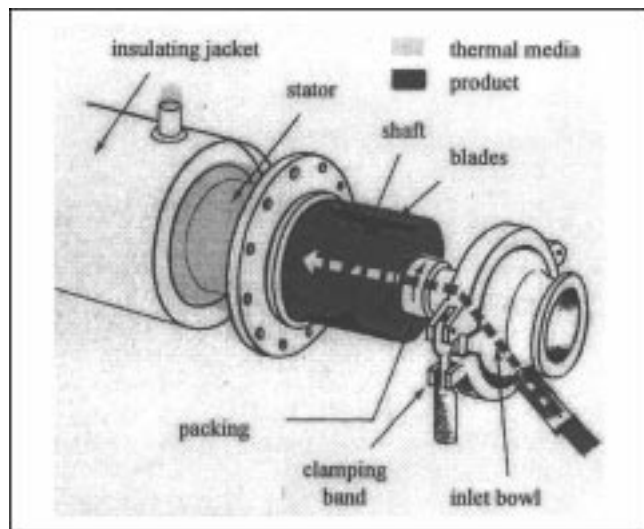


Figure 1. Principal design of SSHE. (Courtesy of Duprat Company.)

al., 1987). Depending on the rotational speed of the rotor, two different flow regimes exist: laminar and vortical flow. But, if in the case of the annulus, the change between these two regimes occurs for a critical value of Taylor number ($Ta_g \approx 40$) increasing with Re_{axg} (DiPrima, 1960), it is much more difficult, in the case of SSHE, to suggest a critical value of Ta_g corresponding to the formation of Taylor vortices. Investigating the transition between laminar flow and vortical flow is important from an industrial point of view, because it promotes efficient mixing and limits rotational speed. Indeed, the mechanical fragility of treated products will sometimes lead to working constraints, thereby reducing rotational speed. Yet, no direct measurement of the wall shear rate in SSHE is available today. Only a few studies (Leuliet et al., 1986; Maingonnat et al., 1987; Härröd, 1990) using indirect methods (pressure drop or evaluation) exist.

A preliminary study of the flow inside a SSHE has been investigated using the thermal evolution of model Newtonian and non-Newtonian fluids in heating or cooling conditions (Dumont et al., 2000). The study shows that the presence of the blades should promote the appearance of instabilities at lower values of generalized Taylor number ($Ta_{gc} = 10$ with blades, and $Ta_{gc} = 39$ without blades). However, these first results must be confirmed by other investigations. In a recent work (Dumont, 1999a), we used a visualization technique and electrodiffusion probes to measure the wall shear rate in order to get a realistic representation of flow conditions inside a scale-down model of the exchanger. The experimental study,

based on the electrodiffusion technique, represents a challenge in the special case of SSHE because of the scraping of the probe's surface by the blades. The transition between laminar and vortex flow occurs for a critical value of Taylor number ($Ta_{gc} \approx 80$) greater (Dumont, 1999a) than the one determined in annulus ($Ta_{gc} \approx 45$), and the wall shear rates measured in SSHE are compared and discussed with those of the literature (Leuliet et al., 1986; Maingonnat et al., 1987; Härröd, 1990).

In this article, particular attention is given to ways the blades scrape the electrochemical probes. The evolution of the limiting diffusion current given by the probes in scraping modes is presented in the case of highly viscous Newtonian fluids and in the case of non-Newtonian model fluids. Because of the unsteady flow, the interpretation of electrodiffusion measurements is realized using different ways of calculating the wall shear rate. Results given by each method are presented, discussed, and compared.

Experimental Details

Scale-down model of SSHE

The present work was carried out on a scale-down model of the Duprat TR 13x60 industrial exchanger. All dimensions are given in Table 1. The scale-down model was built in order to present the same thermal behavior as that of the industrial SSHE (Dumont et al., 1999b). The design principle used was to achieve the Ta_g order of magnitude found in the industrial exchanger ($0 < Ta_g < 100$) when keeping rotational speed at industrial values ($0 < N < 10 \text{ s}^{-1}$). The shaft and stator diameters were chosen to be half the ones of the industrial apparatus (which keeps a constant d_r/d_s ratio). The exchanger volume was calculated taking into account the axial flow velocity, which was chosen, for a given flow rate, in order to keep the same residence time as in the industrial apparatus. The stator length determined by this method (Table 1) represented a compromise on a half-scale of two different lengths commonly used in the food industry ($L/d_s \approx 2.3\text{--}7.7$). The pilot plant included an inlet tank, a pump, the scale-down model of the exchanger, an electromagnetic flowmeter Promag (Endress + Hauser), and an experimental apparatus for the electrochemical technique.

Electrochemical method

Wall shear rates studies were conducted at isothermal conditions ($T = 25^\circ\text{C}$). The limiting diffusion current was measured on twelve 0.4-mm-diameter circular microelectrodes embedded axially on the outer cylinder surface (Figure 2). The stainless-steel shaft served as the auxiliary electrode and the well-known ferri-, ferrocyanide system ($\text{Fe}(\text{CN})_6^{3-} + e^- \leftrightarrow \text{Fe}(\text{CN})_6^{4-}$) was used with a large excess of supporting

Table 1. Geometrical Characteristics of Industrial SSHE and Its Scale-Down Model

	Industrial SSHE (1)	Scale-Down Model (2)	Ratio (1)/(2)
Stator diameter (d_s)	0.13 m	0.065 m	2
Stator length (L)	0.60 m	0.38 m	1.58
Ratio (L/d_s)	4.61	5.85	0.79
Rotor diameter (d_r)	0.080 m	0.040 m	2
Ratio (d_r/d_s)	0.615	0.615	1
Gap $e = (d_s - d_r)/2$	0.025 m	0.0125 m	2
Exchange surface	0.245 (m^2)	7.76×10^{-2} (m^2)	3.16

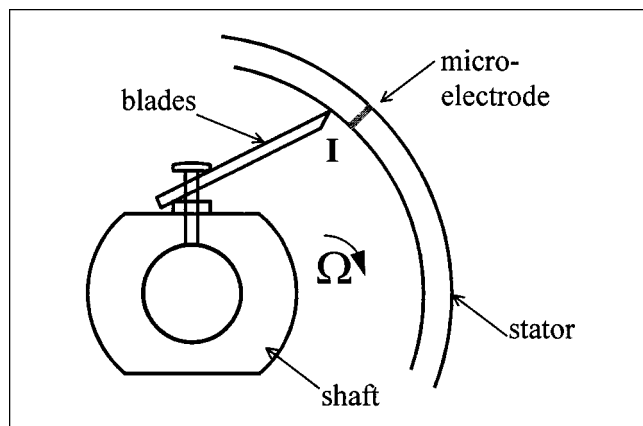


Figure 2. Microelectrode embedded on the outer cylinder.

electrolyte K_2SO_4 so as to eliminate the migration current due to the electric field. Data acquisition and experiment control of the limiting current measurement were carried out with a numerical recorder (Digital Audio Tape Tekelec RD-145T) with 16 channels, which allowed simultaneous recordings. The sampling frequency of the recording was 6000 Hz. Calibration of the probes was performed using the well-defined shear flow (such as Couette flow) and the voltage-step transient experiment (Sobolík et al., 1998).

Three polymeric solutions were used to carry out the experiments: one Newtonian fluid and two shear-thinning fluids. The viscosity measurements were performed at 25°C with

a Couette rheometer TA Instrument AR 1000 with prescribed torque. The fluids were chosen with particular care. Indeed, it was difficult to make highly viscous solutions complying with restraints of the electrochemical method and with our food objectives (dissolution of salts in sufficient quantities, chemically inert fluid, and food products). Emkarox HV 45 (from ICI) is a mixture of polypropylene glycol and polyethylene glycol. The dynamic viscosity of the pure product is equal to 3.7 Pa·s at 25°C. The electrolyte consisted of a mixture of potassium ferricyanide, potassium ferrocyanide, and potassium sulfate as supporting electrolyte. The viscosities of the different aqueous solutions are given in Table 2. We also studied a low-viscosity solution made with polyethylene glycol 35000 (PEG). The Newtonian behavior of these solutions was checked.

Aqueous solutions of carboxymethylcellulose (CMC, from Sigma) exhibit pseudoplastic behavior. Non-Newtonian characteristics depend on the CMC concentration. CMC powder was progressively added to agitated cold water. After the carboxymethylcellulose sodium salt was solubilized, potassium sulfate and potassium ferri- and ferrocyanide were added to the electrolyte. The rheological behavior was modeled by two different power laws, according to the shear rate domains: 5–80 s^{-1} and 50–1230 s^{-1} . The physical properties of the CMC electrolyte are given in Table 3.

The preparation of guar gum solutions was similar to that of the CMC solutions, except that the guar gum dissolution was carried out at 40°C. Two power-law equations were proposed to model the non-Newtonian behavior of guar gum solutions: one where the shear rate, $\dot{\gamma}$, varied from 2 s^{-1} to 20 s^{-1} , and the second for $\dot{\gamma}$ between 10 and 1230 s^{-1} . Rheolog-

Table 2. Physical Properties of Emkarox HV45 Solutions at 25°C

Solution	Water (w/w)	$K_3[Fe(CN)_6]$ ($mol \cdot m^{-3}$)	$K_4[Fe(CN)_6]$ ($mol \cdot m^{-3}$)	K_2SO_4 ($mol \cdot m^{-3}$)	ρ ($kg \cdot m^{-3}$)	μ (Pa·s)	D $10^{10}(m^2 \cdot s^{-1})$
HV45-80	20%	5.327	5.327	106.5	1080	1.18	0.51
HV45-75	25%	5.304	5.304	127.3	1079	0.84	0.70
HV45-70	30%	5.283	5.283	158.5	1077	0.60	0.82
HV45-65	35%	5.262	5.262	210.5	1073	0.43	1.00
HV45-60	40%	5.241	5.241	209.6	1071	0.32	1.15
HV45-55	45%	5.220	5.220	229.7	1070	0.23	1.35
PEG	—	5.000	5.000	250.0	1058	0.04	3.50

Table 3. Physical Properties of CMC and Guar Solutions at 25°C

Solution Wt. (%)	ρ ($kg \cdot m^{-3}$)	$K_3[Fe(CN)_6]$ ($mol \cdot m^{-3}$)	$K_4[Fe(CN)_6]$ ($mol \cdot m^{-3}$)	K_2SO_4 ($mol \cdot m^{-3}$)	D $10^{10}(m^2 \cdot s^{-1})$	Shear Rate Domain $\dot{\gamma}$ (s^{-1})			
						5–80		50–1,234	
						n	K (Pa·s n)	n	K (Pa·s n)
CMC 0.5%	1046	5.0	5.0	300	7.50	0.85	0.11	0.73	0.16
CMC 0.7%	1071	5.0	5.0	500	7.50	0.78	0.36	0.65	0.63
CMC 0.9%	1047	5.0	5.0	300	7.50	0.70	1.05	0.55	1.98
CMC 1.0%	1047	4.0	4.0	300	7.50	0.66	1.64	0.51	3.02
CMC 1.1%	1048	4.0	4.0	300	7.50	0.62	2.49	0.48	4.44
						Shear Rate Domain $\dot{\gamma}$ (s^{-1})			
						2–20		10–1,234	
						n	K	n	K
Guar 0.7%	1046	3.0	3.0	300	6.90	0.65	0.78	0.47	1.31
Guar 0.8%	1046	4.0	4.0	300	6.90	0.63	1.21	0.44	2.04
Guar 1.0%	1043	5.0	5.0	300	6.90	0.51	3.29	0.36	4.86
Guar 1.2%	1047	5.0	5.0	300	6.90	0.44	6.40	0.32	8.91

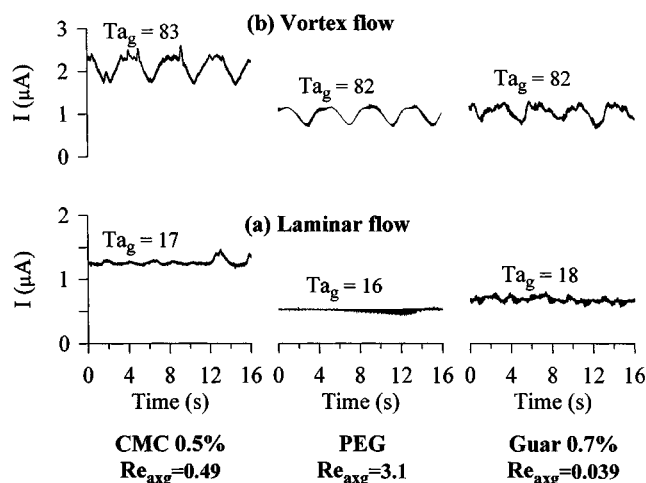


Figure 3. Record of limiting diffusion current with respect to time in annulus for three different solutions ($Q = 35 \text{ L} \cdot \text{h}^{-1}$).

ical data are summarized in Table 3. The diffusion coefficients of ferricyanide ions (Table 3) in these polymeric solutions were determined by different experimental methods (Legrand et al., 2000).

Each experiment was performed in the following way: flow rate ($Q = 35 \text{ L} \cdot \text{h}^{-1}$), rotational speed of the rotor (N varied from 30 rpm^{-1} to 600 rpm^{-1}) and, product temperature ($T = 25^\circ\text{C}$) before the inlet were all adjusted to the desired values. For each rotational speed, the limiting diffusion currents from the microelectrodes were numerically recorded for 90 s (laminar flow) or for 150 s (vortex flow). Generalized axial Reynolds number (Re_{axg}) and generalized Taylor number (Ta_g) were used to characterize the flow pattern.

Results and Discussion

Validation of the electrochemical method in annulus

The experiments were first carried out in the SSHE without blades, which represents an annulus, in order to verify the right running order of the electrochemical technique. The flow stability investigations consisted of determining the dependence of the limiting current value I on the angular velocity Ω of the shaft. At the beginning, the value of I is the same as that for time (Figure 3), which is interpreted as a flow without vortices ($Ta_g < 40$). When a certain value of rotational speed is reached, I suddenly changes. The limiting current value presents a periodical form (Figure 3) attributed to the onset of instability. This result is confirmed by visual experiments carried out with HV45 Emkarox solutions (Dumont, 1999a). As it turns out, onset of the periodic oscillation of the limiting current actually corresponds to the formation of Taylor vortices. In this flow, toroidal vortices surround the inner cylinder and proceed through the annulus without being disturbed by the axial flow. The results obtained for very small values of the axial flow velocity U_d can be applied in analysis stability of Couette flow ($U_d = 0$). Furthermore, the electrochemical method allows us to get continuous axial measurements of wall shear rate on the body of the Taylor cells. Basically, using the limiting diffusion current

to measure the wall shear rate is based on the following assumption: the species transport and measured current are controlled by the velocity field very close to the working probe. In this region, if the length of the microelectrode is very small in the flow direction, the concentration boundary layer on the electrode is thin, and the velocity field inside the concentration boundary layer can be approximated by the linear dependence on the normal distance from the surface, y , with the shear rate, S . Assuming that the limiting current is controlled by convective diffusion only, the mass-transport equation can be written as:

$$\frac{\partial C}{\partial t} + Sy \frac{\partial C}{\partial x} = D \left(\frac{\partial^2 C}{\partial x^2} + \frac{\partial^2 C}{\partial y^2} \right). \quad (1)$$

If the Peclet number ($Pe = SL^2/D$) is sufficiently high (> 5000 ; Ling, 1963), the diffusion term ($\partial^2 C/\partial x^2$) in the flow direction may be neglected. If the flow fluctuations are slow enough, as in Figure 3, the quasi steady state can be applied and Eq. 1 becomes:

$$Sy \frac{\partial C}{\partial x} = D \frac{\partial^2 C}{\partial y^2}. \quad (2)$$

Then, integration of Eq. 2 gives the wall shear rate, S , with respect to the limiting diffusion current, I (Reiss and Hanratty, 1963):

$$S = \left(\frac{1.477}{zF} \right) \frac{I^3}{D^2 C_0^3 d^5}, \quad (3)$$

where z is the number of electrons involved in the redox reaction, F the Faraday constant, d the diameter of the circular microelectrode, C_0 the bulk concentration of the reacting ions, and D the diffusion coefficient of these ions in solution. For a given microelectrode, an example of dimensionless representation of the mean wall shear rate is presented in Figure 4. This representation allows us to detect the tran-

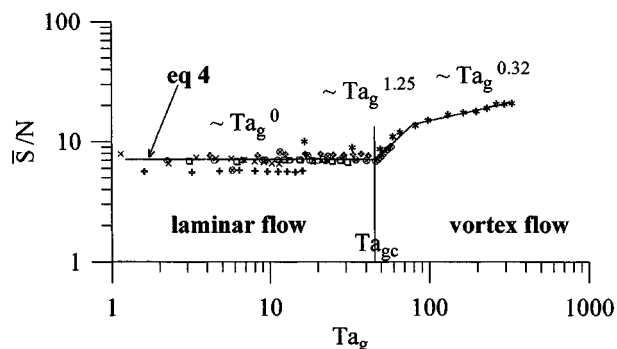


Figure 4. Dimensionless representation of wall shear rates with respect to Ta_g in annulus for Newtonian solutions ($Q = 35 \text{ L} \cdot \text{h}^{-1}$).

(\times): HV45-80; (\oplus): HV45-75; (\circ): HV45-70; (\square): HV45-65; (\diamond): HV45-60; (\otimes): HV45-55; (\ast): PEG.

sition between laminar and vortex flow ($Ta_{gc} \approx 45$) and to verify the theoretical value of the ratio (\bar{S}/N) obtained from the Couette flow velocity profile for a power-law fluid ($n=1$ for a Newtonian fluid) and for laminar flow,

$$\frac{\bar{S}}{N} = \frac{4\pi}{n} \frac{R_r^{2/n}}{(R_s^{2/n} - R_r^{2/n})}. \quad (4)$$

These results corresponding to the flow in annulus confirm that the experimental apparatus and the electrodiffusional diagnostics allow us to obtain satisfying information in the case of particularly viscous Newtonian fluids. The same conclusion can be drawn with non-Newtonian solutions. Therefore, it is possible to work with the blades on the shaft and to pick up the information given by the probes.

Wall shear rates in SSHE (scraping situation)

In the scale-down model of the SSHE, with blades mounted on the inner rotating cylinder, with axial flow and no heat transfer, visual investigations show that the flow is laminar in a wide range of Ta_g (up to 80). For more important values of Ta_g , flow structure presents a vortex pattern, but vortices are hindered by the rotation of the blades (Dumont, 1999a). Figure 5 shows an example of the general evolution of the limiting diffusion current given by the probes with respect to time. The evolution of I is the same for every value of Ta_g and for the different fluids (Figure 6a–6c). These representations indicate that the limiting diffusion current is fully controlled by the blade rotation (for each value of Ta_g). Figure 6d shows that the minimum values of the diffusional current blades is significantly greater than those in an annulus without blades. The vortex flow pattern is repeated each time the blade passes, thus resulting in an unsteady vortex flow, which by nature is different from Taylor vortices. Actually, the scraping of the microelectrodes is very fast and creates large fluctuations. Thus, wall shear rates appear independent of the flow pattern in the apparatus. Figures 5 and 6 also show that the electrodiffusion technique is efficient in the specific case of scraping conditions. The gap between the edge of the blades and the stator is therefore more important than the thickness of the mass-transfer boundary layer. However, at those times when the blades buckle, the clearance between

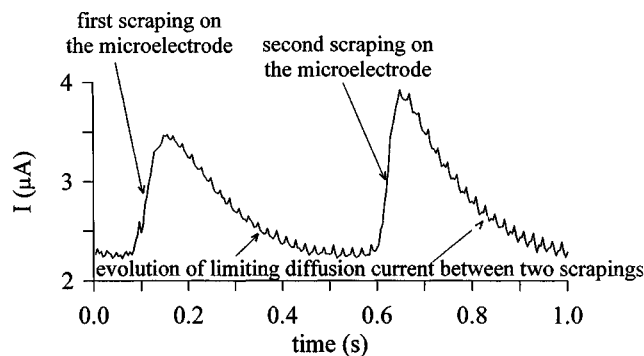


Figure 5. Evolution of limiting diffusion current with time in scraping situation (non-Newtonian solution of 0.5% CMC; $Re_{axg} = 0.5$; $Q = 35 \text{ L} \cdot \text{h}^{-1}$).

the edge of the blade and the wall may sometimes become so thin that no electrolyte occurs on the microelectrode. In this case, a short power cut is recorded (Figure 7).

Generally, when the blades are scraping without power cut, the very fast, large fluctuations of the limiting diffusion current do not allow us to calculate the wall shear rates using Eq. 3. Indeed, the instantaneous wall shear rate can be related to the instantaneous limiting current only in the case of quasi-steady flows. Interpretation of the electrodiffusion measurements is difficult mainly because it is necessary to consider the dynamic response to flow fluctuations of the concentration boundary layer at the probe surface. This response was investigated in the time as well as in the frequency domains. The frequency analysis, dealing with linear theory of small fluctuations (Nakoryakov et al., 1986; Deslouis et al., 1990), allows correction of the experimentally obtained power spectra of the electrodiffusion current signal in order to calculate the wall velocity gradient power spectra or to predict its amplitude attenuation and phase shift. In the time-domain analysis, the aim was to obtain a direct correction of the electrodiffusion signal in order to solve the problem of the boundary layer and to restore the wall shear rate from the measured current. Sobolík et al. (1987) studied the dynamic response of a microelectrode with periodic wall shear rate evolutions. These authors solved the mass-balance equation, assuming that the concentration field is a similar function of the three variables:

$$C(x, y, t) = C_0 \left(1 - F \left(\frac{y}{\delta_i(t)} \left(\frac{d}{x} \right)^{1/3} \right) \right) \quad (5)$$

where $F(\zeta)$ is a decreasing function that is normalized by the conditions $F(0) = 1$, $F(\infty) = 0$ and $F'(0) = -1$. Substitution of Eq. 5 into the transport equation,

$$\frac{\partial C}{\partial t} + Sy \frac{\partial C}{\partial x} = D \frac{\partial^2 C}{\partial y^2}, \quad (6)$$

and the integration over the whole concentration boundary layer led to the following expression for the time history of the wall shear rate $S_c(t)$:

$$S_c(t) = S(t) + \frac{2}{3} t_0 \left(\frac{\partial S}{\partial t} \right), \quad (7)$$

where $S_c(t)$ is the value of the wall shear rate corrected with respect to the probe inertia, $S(t)$ is the quasi-steady interpretation of the measured limiting diffusion current (Eq. 3), and t_0 is the characteristic time of the microelectrode corresponding to the intersection of both asymptotical parts of the current response to the transient step change of the polarization potential (Sobolík et al., 1998):

$$t_0 = 0.428 \left(\frac{d^2}{DS^2} \right)^{1/3}. \quad (8)$$

Wavy film flow experiments (Sobolík et al., 1987), using simultaneous measurements of film thickness and wall shear stress, demonstrate that the time-domain correction Eq. 7

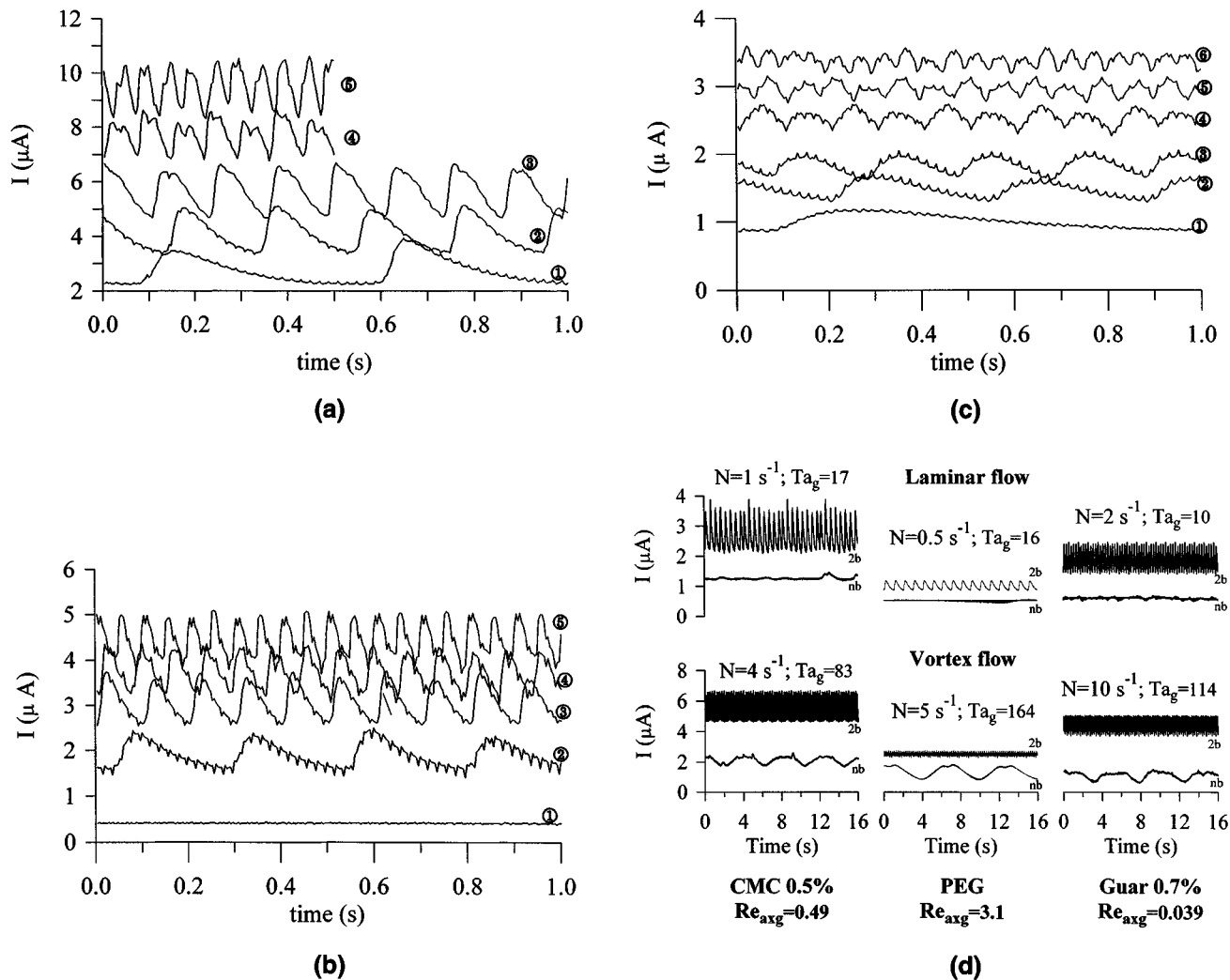


Figure 6. Evolution of limiting diffusion current with time.

(a) For a non-Newtonian solution of 0.5% CMC in SSHE ($Re_{axg} = 0.5$; $Q = 35 \text{ L}\cdot\text{h}^{-1}$). ①: $Ta_g = 15$, $N = 1 \text{ s}^{-1}$; ②: $Ta_g = 48$, $N = 2.5 \text{ s}^{-1}$; ③: $Ta_g = 88$, $N = 4 \text{ s}^{-1}$; ④: $Ta_g = 179$, $N = 7 \text{ s}^{-1}$; ⑤: $Ta_g = 282$, $N = 10 \text{ s}^{-1}$. (b) For a non-Newtonian solution of 0.7% guar gum in SSHE ($Re_{axg} = 0.04$; $Q = 35 \text{ L}\cdot\text{h}^{-1}$). ①: $Ta_g = 0$, $N = 0 \text{ s}^{-1}$; ②: $Ta_g = 10$, $N = 2 \text{ s}^{-1}$; ③: $Ta_g = 40$, $N = 5 \text{ s}^{-1}$; ④: $Ta_g = 66$, $N = 7 \text{ s}^{-1}$; ⑤: $Ta_g = 114$, $N = 10 \text{ s}^{-1}$. (c) For a Newtonian solution of PEG in SSHE ($Re_{axg} = 3.1$; $Q = 35 \text{ L}\cdot\text{h}^{-1}$). ①: $Ta_g = 16$, $N = 0.5 \text{ s}^{-1}$; ②: $Ta_g = 49$, $N = 1.5 \text{ s}^{-1}$; ③: $Ta_g = 82$, $N = 2.5 \text{ s}^{-1}$; ④: $Ta_g = 164$, $N = 5 \text{ s}^{-1}$; ⑤: $Ta_g = 230$, $N = 7 \text{ s}^{-1}$; ⑥: $Ta_g = 328$, $N = 10 \text{ s}^{-1}$. (d) In annulus for three different solutions with and without blades ($Q = 35 \text{ L}\cdot\text{h}^{-1}$). nb: no blades; 2b: with 2 blades.

gives satisfactory results. New experimentation, based on wavy film flow, led Tihon and Sobolík (1993) to show that Eq. 7 enables the restoration of the instantaneous wall shear rate from the measured current even at large flow fluctuations. In the case where annular flows are developed, Tihon et al. (1995) establish that, in spite of the slow flow fluctuations, the inertia correction is significant, especially in the parts of the signal where the limiting current diffusion changes more quickly (great values of dI/dt). Furthermore, Tihon et al. (1995) demonstrated that the direct correction of the measured signal made in the time domain provides spectral results that are very similar to the correction made in the frequency domain (Nakoryakov et al., 1986), and gives reliable, undistorted information on the wall shear rate, even in complex flow conditions.

In the case of SSHE, it is possible to use Eq. 7 to calculate the wall shear rate with respect to time; but first it is neces-

sary to model the $S(t)$ signal calculated using Eq. 3. Figure 8 presents an example of the wall shear rate evolution first calculated with Eq. 3, supposing the quasi-steady flow, and second, with Eq. 7, giving the corrected wall shear rate $S_c(t)$ for a 0.5% CMC solution with $N = 1 \text{ rev/s}$. This rotational speed corresponds to the lowest frequency (2 Hz) of the fluctuations. Particular attention must be paid to determining the maximal values (S_{max}) of $S(t)$ and $S_c(t)$ corresponding to the scraping situation. Indeed, S_{max} values allow us to deduce an order of magnitude of the clearance between the edge of the blade and the tube wall. Figure 8 shows that maximal values of $S(t)$ and $S_c(t)$ are, respectively, 375 and 612 s^{-1} , which represents a difference of 63%. This example clearly shows the importance of the dynamics of the flow pattern, even in the favorable case of slow rotational speed. For greater rotational speeds, the blades' passage time on the surface of the probes decreases, and (dS/dt) increases as a consequence.

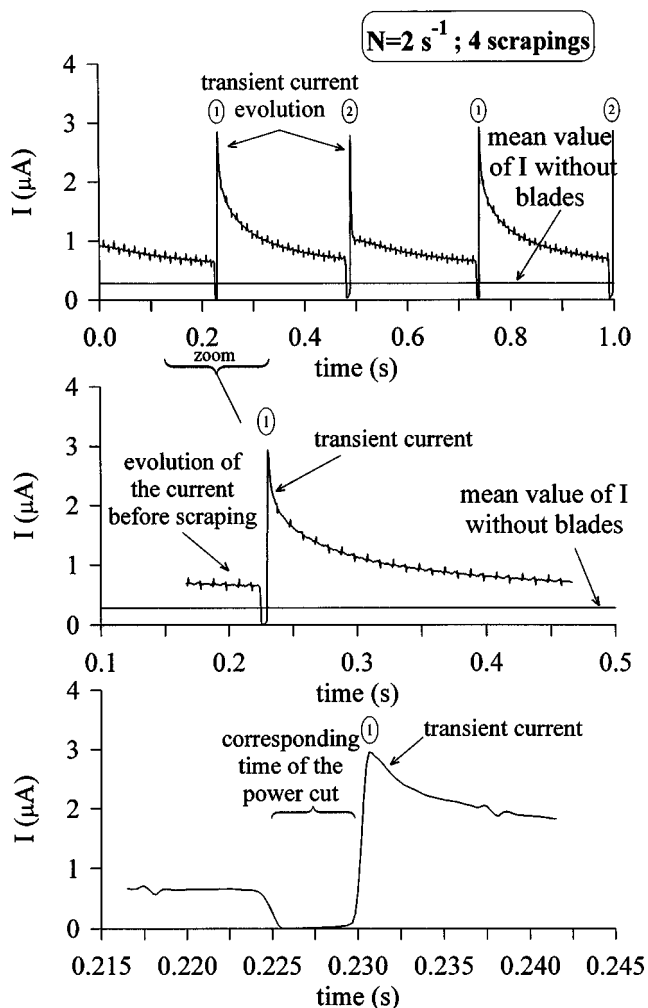


Figure 7. Evolution of I with respect to time for a Newtonian solution of HV45-80 when contact exists between the edge of the blade and the wall tube.

The correction is then difficult to calculate accurately, and the difference between the maximal values of $S(t)$ and $S_c(t)$ increases progressively. Finally, this example, which corresponds to a favorable situation, illustrates the difficulty of this specific calculation in the case of the scraping situation ($dS/dt \rightarrow \infty$).

Another approach to an analytical calculation of the wall shear rate in unsteady state was investigated. The evolutions of the limiting current diffusion presented in Figures 5 and 6 show that the effects on the probes of the blades passing can be compared with the effects of a pulsating flow (Tsochatzidis and Karabelas, 1994; García-Antón et al., 1997). In the case of an unsteady-state pulsating flow, where the limiting current is influenced by the pulsation amplitude (S_p) and the pulsation frequency (ω), Martemianov and Sviridov (1989) developed a procedure to calculate the size of Faradaic rectification. This quantity is defined as the period-average excess of current in the pulsating flow over the current in the quiescent electrolyte. These authors indicated that the diffusate concentration distribution in a flow fluctuating harmonically

Modeled curves:

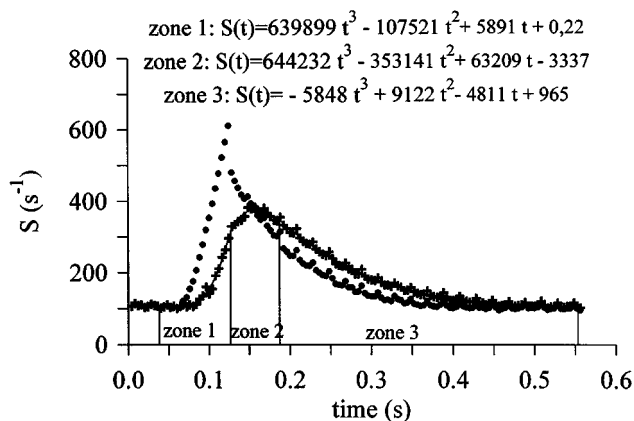


Figure 8. Example of evolution of the wall shear rates S (steady-state) and S_c (corrected) with time for a 0.5% CMC solution ($N = 1 \text{ s}^{-1}$).

(+): $S(t)$ calculated using Eq. 3; (—): modeled curves of $S(t)$; (●): $S_c(t)$ calculated using Eq. 7.

was described by the transient convective diffusion equation:

$$\frac{\partial C}{\partial t} + S_p y \cos \omega t \frac{\partial C}{\partial x} = D \frac{\partial^2 C}{\partial y^2}. \quad (9)$$

Martemianov and Sviridov (1989) introduced the dimensionless variables in order to solve Eq. 9:

$$\bar{x} = \frac{x}{l}; \quad \bar{y} = \frac{y}{\delta_m}; \quad \bar{t} = t\omega; \quad \delta_m = \left(\frac{Dl}{S_p} \right)^{1/3};$$

$$\bar{\omega} = \frac{\omega \delta_m^2}{D}; \quad \bar{C} = \frac{C}{C_s} \quad (10)$$

where l is the characteristic dimension of the microelectrode along the direction of the velocity fluctuations. Equation 9 becomes

$$\bar{\omega} \frac{\partial \bar{C}}{\partial \bar{t}} + \bar{y} \cos \bar{t} \frac{\partial \bar{C}}{\partial \bar{x}} = \frac{\partial^2 \bar{C}}{\partial \bar{y}^2}, \quad (11)$$

with

$$\bar{\omega} = \omega \left(\frac{l^2}{DS_p^2} \right)^{1/3} \quad (12)$$

and the following boundary conditions:

$$\begin{aligned} \bar{C} &= 0 && \text{at the surface of the probes} \\ \left(\frac{\partial \bar{C}}{\partial \bar{y}} \right)_{\bar{y}=0} &= 0 && \text{no mass transport at the insulator surface} \\ \bar{C} &= 1 && \text{in the flow } (\bar{y} \rightarrow \infty). \end{aligned} \quad (13)$$

Returning to dimensional quantities, Martemianov and Sviridov (1989) obtained the Faradaic current rectification, \bar{I} :

$$\bar{I} = zFD \frac{C_s}{\delta_m(l)} \Psi(\bar{\omega}) A. \quad (14)$$

The expression of the dimensionless function Ψ according to $\bar{\omega}$ is discussed below:

1. $\bar{\omega} \ll 1$: The fluctuations are characterized by low frequencies, and the diffusional regime corresponds to the quasi-steady mode. At any time the current $I(t)$ can adjust the changes in the wall shear rate. Then, the function Ψ is independent of $\bar{\omega}$, and \bar{I} is proportional to I :

$$\bar{I} = \beta I \quad \text{with} \quad \beta = \frac{2}{\pi} \int_0^{\pi/2} (\cos t)^{1/3} dt \approx 0.823. \quad (15)$$

2. $\bar{\omega} \gg 1$: For the high-frequency limit of function Ψ , the magnitude of Faradaic current rectification is assumed to be independent of the probe length l along the flow. In this case, the frequency dependence of function Ψ is given by using Eq. 14:

$$\Psi(\bar{\omega}) = \frac{1}{\bar{\omega}} \quad (16)$$

and:

$$\bar{I} = zFAC_s \frac{DS_p}{\omega l}. \quad (17)$$

According to Eq. 12, this calculating procedure assumes that the value of S_p is known *a priori* in order to determine $\bar{\omega}$.

In the special case of SSHE, the fluctuations of the limiting diffusion current with pulsation frequency ($1/2 N$) correspond to a cosine function for high values of N ($N \geq 2.5 \text{ s}^{-1}$) (Figure 9). Our approach first consists of verifying the applicability of Martemianov and Sviridov's procedure for making the calculations. We consider that the passages of the blades on the probes create periodic fluctuations defined as $\cos(\omega t)$, with $\omega = 4\pi N$. First, using Eq. 15 and assuming that condition $\bar{\omega} \ll 1$ is satisfied, we calculate the maximal values of the wall shear rate (S_{\max}). The determination, *a posteriori*, of $\bar{\omega}$ using Eq. 12 with the value of S_{\max} obtained, allows us to verify the validity of the procedure for making the calculations. The same operation is performed assuming that condition $\bar{\omega} \gg 1$ is satisfied. In this case, S_{\max} is calculated using Eq. 17. Figure 10 displays examples of S_{\max} evolutions calculated with respect to Ta_g using Eqs. 15 and 17; evolutions of the wall shear rates, S_{\max} , calculated assuming a quasi-steady state (Eq. 3) and corrected with the probe inertia (Eq. 7), are also presented. Table 4 contains the limits of $\bar{\omega}$ variations determined *a posteriori* for every solution and rotational speed.

For Newtonian solutions, Table 4 shows that the $\bar{\omega}$ calculation *a posteriori* does not allow confirmation of the assumption made for the S_{\max} calculation. In the first case (hypothesis corresponding to $\bar{\omega} \ll 1$), $\bar{\omega}$ values are generally greater than 1, and in the second case (hypothesis corresponding to $\bar{\omega} \gg 1$), these values frequently appear to be less than 1.

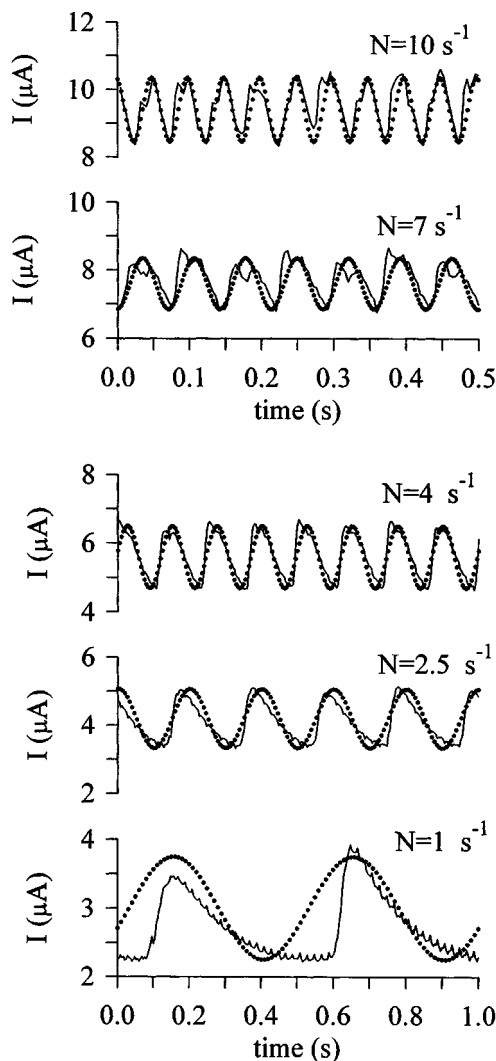


Figure 9. Comparison of the experimental signal (—) with a $\cos(4\pi Nt)$ function (●) for a 1.2% guar gum solution ($N = 1 \text{ s}^{-1}$).

Therefore, conditions linked to the S_{\max} calculating procedure are not satisfied. We establish that $\bar{\omega} \approx 1$, which demonstrates that flow fluctuations generated by the passages of the blades are too rapid to consider that quasi-steady state occurs and too slow to neglect the probe length along the flow in order to apply the calculating procedure given by Eq. 16. In all events, the working of the SSHE represents an intermediate case between these two extreme situations and the actual wall shear rate must exist between the S_{\max} values given by these extremes.

Figure 10a shows the different S_{\max} evolutions for a Newtonian solution. Since the assumption of the quasi steady state cannot be applied, the actual wall shear must be higher than the evolution corresponding to the \circ symbols. In the case of the corrected wall shear rate $S_c(t)$, using the derivative of the mathematical function modeling the experimental data leads us to obtain high values of S_{\max} , because the passage of the blade on the probe surface corresponds to a very sharp increase in the limiting diffusion current. Consequently, the

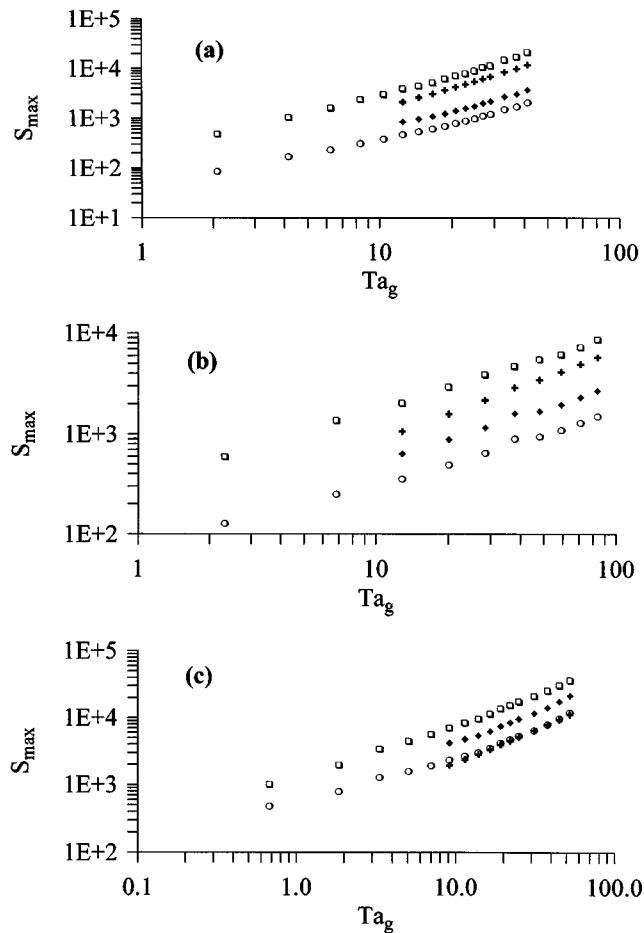


Figure 10. Examples of S_{\max} evolution with respect to Ta_g for the following solutions.

(a) HV45-60; (b) guar gum 0.8%; and (c) CMC 0.9%. (○): S_{\max} calculated assuming quasi-steady state (Eq. 3); (□): corrected wall shear rates (Eq. 7); (◆): S_{\max} calculated assuming $\bar{\omega} \ll 1$ (Eq. 15); (+): S_{\max} calculated assuming $\bar{\omega} \gg 1$ (Eq. 17).

S_{\max} evolution represented by the □ symbols certainly constitutes the upper limit of these wall shear rates. The wall shear rates evolution, assuming $\bar{\omega} \ll 1$ (◆) and assuming $\bar{\omega} \gg 1$ (+), is logically located between the quasi-steady evolution and the corrected wall shear rate. Thus, we found that Figure 10a agrees relatively well with the expected evolution of the values of the maximum wall shear rate according to the assumptions of the different models. In particular, the two *a priori* more appropriate models (Eq. 7 and Eq. 17) give very similar results (Figure 10a).

For non-Newtonian guar gum solutions, it seems possible, with respect to the $\bar{\omega}$ values given by Table 4, to apply the comments developed for Newtonian solutions (Figure 10b). Table 4 shows that there is a difference between guar gum solutions and CMC solutions. The $\bar{\omega}$ calculating procedure, derived from S_{\max} values obtained assuming that $\bar{\omega} \ll 1$ is satisfied, shows that $\bar{\omega}$ is indeed inferior to 1, though the assumption $\bar{\omega} \ll 1$ is not actually verified. In that case, the diffusional mode should be near the quasi steady state. Specifically, this behavior is observed on Figure 10c: first, by

Table 4. Calculated Values of $\bar{\omega}^*$

Solutions	First Case: S_{\max}	Second Case: S_{\max}
	Calc. Assuming $\bar{\omega} \ll 1$ (Eq. 15)	Calc. Assuming $\bar{\omega} \gg 1$ (Eq. 17)
	$\bar{\omega}$ Values Calc. <i>a posteriori</i> from S_{\max}	
HV45-80	0.54–3.63	0.23–2.02
HV45-75	0.56–3.51	0.23–2.00
HV45-70	0.49–4.13	0.22–3.34
HV45-65	0.44–3.53	0.21–3.17
HV45-60	0.48–3.94	0.22–3.29
HV45-55	0.41–3.41	0.21–3.14
PEG	0.63–4.14	0.24–3.35
CMC 0.5%	0.09–0.89	0.13–2.01
CMC 0.7%	0.09–0.84	0.13–1.96
CMC 0.9%	0.08–0.67	0.12–1.82
CMC 1.0%	0.08–0.39	0.12–0.96
CMC 1.1%	0.06–0.34	0.11–0.91
Guar 0.7%	0.13–1.46	0.14–2.37
Guar 0.8%	0.32–1.66	0.19–1.56
Guar 1.0%	0.20–0.99	0.17–1.31
Guar 1.2%	0.53–1.37	0.23–1.47

* Determination of the variation limits of $\bar{\omega}$ for each solutions ($T = 25^\circ\text{C}$). In the whole cases, the minimal value of $\bar{\omega}$ is obtained for $N = 10 \text{ s}^{-1}$ ($\omega = 125.6 \text{ Hz}$), and the maximal value of $\bar{\omega}$ is obtained for the smallest rotating speed ($N = 0.5 \text{ s}^{-1}$ corresponding to $\omega = 6.28 \text{ Hz}$ or $N = 1 \text{ s}^{-1}$ corresponding to $\omega = 12.56 \text{ Hz}$).

an S_{\max} evolution (◆) included between the one of the wall shear rates calculated assuming the quasi steady state and that of the corrected wall shear rates; and secondly, by an aberrant S_{\max} evolution calculated assuming $\bar{\omega} \gg 1$ (+).

However, these comments concerning the actual evolution of the wall shear rate are based on a great number of assumptions, which only allows a rather good estimation of the actual S_{\max} value. Finally, our study reveals that in the scraping situation generated by using the SSHE, it is not possible to find an analytical solution to the convective diffusion equation that allows us to calculate the wall shear rate from the experimental measurements of the mass transport at the probes surface. Only a numerical-based mode of calculation, based on the inverse method, should be able to give the values of the wall shear rate. Studies specifically based on this problem (Mao and Hanratty, 1991, 1992) show that the goal can be accomplished in the case of large-amplitude unsteady flows.

From the maximum value of the wall shear rate in the SSHE, it is possible to estimate the clearance (δ) between the edge of the blades and the tube wall. Assuming that the velocity profile between scraper blade and tube wall is linear, the wall shear rate is given by the following equation:

$$S_{\max} = \frac{2\pi R_s N}{\delta} \quad (18)$$

Figures 11 and 12 show a dimensionless representation of the evolutions of the wall shear rate calculated assuming the quasi steady state (Eq. 3) and the corrected wall shear rate S_c calculated using Eq. 7 for the Newtonian and non-Newtonian solutions, respectively. As a comparison, these figures also display the evolution of the ratio (\bar{S}/N) obtained without blades. Figures 11 and 12 clearly show that the wall shear

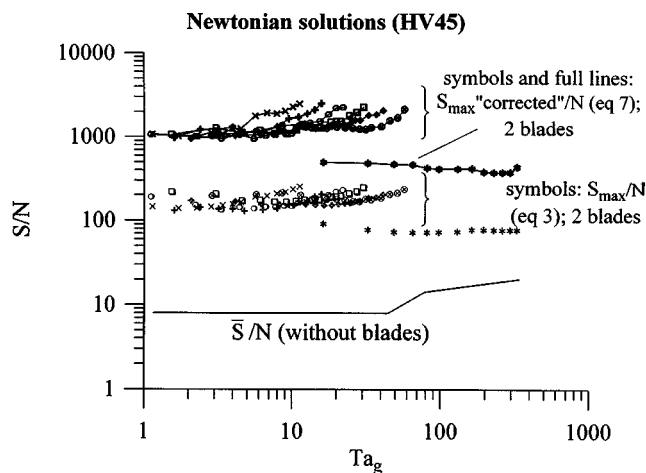


Figure 11. Evolution of S_{\max}/N (calculated from both Eq. 3 and Eq. 7) with respect to Ta_g for Newtonian solutions in SSHE.

Comparison with (\bar{S}/N) measured in annulus. (X): HV45-80; (⊕): HV45-75; (○): HV45-70; (□): HV45-65; (◇): HV45-60; (⊗): HV45-55; (*): PEG.

rates in the SSHE are noticeably different from those observed in the annulus. Three observations should be mentioned. First, wall shear rates in the SSHE (S_{\max}) are much more important (10 to 100 times higher) than those measured in the annulus under the same conditions. Second, the transition between laminar and vortex flow in the scraping situation cannot be determined, which agrees with the visual observations (Dumont, 1999a). Third, evolution changes in the S/N ratio (S_{\max}/N) appear for low and variable values of Ta_g , as per the rheological properties of the solutions. Phenomena such as viscous heating of the liquid between the edge of the scraper blade and the wall, which should be considerable (Trommelen and Beek, 1971b), might explain these shifts. The specific properties of the solutions (slip effect) may also be considered. Experimental determination of S_{\max}/N (Figures 11 and 12) allows us to calculate δ using Eq. 18. The lowest value of δ calculated in this way is equal to 50×10^{-6} m. Nevertheless, in the case of blade deformation (buckling), δ might locally be lower than this value.

Conclusion

The use of electrochemical probes remains a successful method for investigating the evolution of the wall shear rate in complex geometries such as SSHE. Unlike wall shear rates in an annulus, which depend on the flow regime, the shear rate on the stator wall of a SSHE seems fully controlled by blade rotation. Thus, wall shear rates appear ten to a hundred times greater in a SSHE than in an annulus. In these conditions, the lowest value of the clearance between the edge of the blades and the stator is about 50×10^{-6} m. But in a specific scraping situation of a electrochemical probe by a blade, our study shows that the relationship between the wall shear rate and the measurements of mass transport on the probe is not a trivial problem. In fact, the use of an analytical solution corresponding to the quasi steady state leads to erroneous values of the wall shear rate. However, the wall shear rate at the scraping surface can be estimated either by analyzing the concentration field variations near the probe in order to take probe inertia into account (Sobolík et al., 1987), or by resolving the convective diffusion equation in the case of periodic flows. The next step of the study will be the numerical determination of the wall shear rate from electrochemical probes by using an inverse method.

Conclusion

Notation

$$Re_{\text{axg}} = \frac{\rho U_d^{2-n} d_h^n}{K}$$

$$Ta_g = \sqrt{\frac{R_s - R_r}{R_r}} \frac{\rho d_h^n}{2^n} \frac{(\Omega R_r)^{2-n}}{K}$$

\bar{S} = average wall shear rate in an annulus, s^{-1}
 C = dimensionless concentration
 \bar{t} = dimensionless time
 A = surface area of the probe, m^2
 C = concentration, $mol \cdot m^{-3}$
 d_h = hydraulic diameter, m; $d_h = (d_s - d_r)$
 e = gap, m
 K = consistency coefficient of the product, Ostwald law, $Pa \cdot s^n$
 L = stator length, m
 n = flow behavior index of the product, Ostwald law
 R_r = rotor radius, m
 R_s = stator radius, m
 S_m = wall shear rate at the inflow boundary in an annulus, s^{-1}
 S_M = wall shear rate at the outflow boundary in an annulus, s^{-1}
 S_p = wall shear rate, s^{-1}
 $\bar{\omega}$ = dimensionless frequency
 β = constant
 δ = clearance between the edge of the blade and stator, m
 δ_m = thickness corresponding to Eq. 10
 δ_r = thickness of diffusional layer at rear edge of the probe, m
 μ = dynamic viscosity for Newtonian fluid, $Pa \cdot s$
 ρ = density, $kg \cdot m^{-3}$

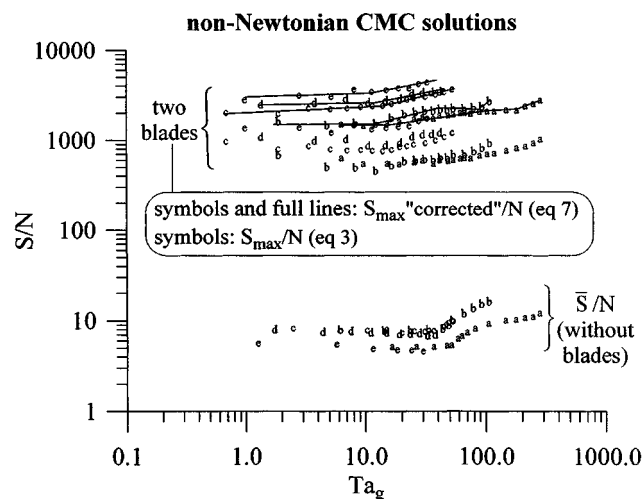


Figure 12. Evolution of S_{\max}/N (calculated from both Eq. 3 and Eq. 7) with respect to Ta_g for non-Newtonian CMC solutions in SSHE.

Comparison with (\bar{S}/N) measured in annulus. (a): 0.5% CMC; (b): 0.7% CMC; (c): 0.9% CMC; (d): 1.0% CMC; (e): 1.1% CMC.

Literature Cited

- Abichandani, H., S. C. Sarma, and D. R. Heldman, "Hydrodynamics and Heat Transfer in Liquid Full Scraped Surface Heat Exchangers. A Review," *J. Food Process Eng.*, **9**, 121 (1987).
- Burmester, S. S. H., P. J. Winch, and A. B. Russell, "A Flow Visualization Technique to Characterize the Mixing in a Scraped Surface Heat Exchanger," *Inst. Chem. Eng. Res. Event.*, **2**, 865 (1996).
- Deslouis, C., O. Gil, and B. Tribollet, "Frequency Response of Electrochemical Sensors to Hydrodynamic Fluctuations", *J. Fluid Mech.*, **215**, 85 (1990).
- DiPrima, R. C., "The Stability of a Viscous Fluid Between Rotating Cylinders with an Axial Flow," *J. Fluid Mech.*, **9**, 621 (1960).
- Dumont, E., "Caractérisation des Ecoulements et des Frottements Pariétaux dans un Echangeur de Chaleur à Surface Raclée," PhD Thesis, Univ. of Nantes, France (1999a).
- Dumont, E., F. Fayolle, and J. Legrand, "Determination of Hydrodynamic Properties in an Industrial Scraped Surface Heat Exchanger and its Scale-down Model", *Récents Progrès en Génie des Procédés*, Ed. Tec-Doc, Lavoisier, **13** (71), 401 (1999b).
- Dumont, E., D. Della Valle, F. Fayolle, and J. Legrand, "Influence of Flow Regimes on Temperature Heterogeneities within a Scraped Surface Heat Exchanger", *J. Food Process Eng.*, in press (2000).
- García-Antón, J., V. Pérez-Herranz, and J. L. Guiñón, "Mass Transfer in an Annular Electrolysis Cell in Pulsating Flow," *J. Appl. Electrochem.*, **27**, 469 (1997).
- Hanratty, T. J., "Use of the Polarographic Method to Measure Wall Shear Stress," *J. Appl. Electrochem.*, **21**, 1038 (1991).
- Härröd, M., "A Literature Survey of Flow Patterns, Mixing, Residence Time Distribution, Heat Transfer and Power Requirements," *J. Food Process Eng.*, **9**, 1 (1986).
- Härröd, M., "Methods to Distinguish Between Laminar and Vortical Flow in Scraped Surface Heat Exchanger," *J. Food Process Eng.*, **13**, 39 (1990).
- Kataoka, K., H. Doi, and T. Komai, "Heat/Mass Transfer in Taylor Vortex Flow with Constant Axial Flow Rates," *Int. J. Heat Mass Transfer*, **20**, 57 (1977).
- Legrand, J., F. Coeuret, and M. Billon, "Structure Dynamique et Transfert de Matière Liquide-Paroi dans le Cas de l'Écoulement Laminaire Tourbillonnaire de Couette-Poiseuille," *Int. J. Heat Mass Transfer*, **26**, 1075 (1983).
- Legrand, J., E. Dumont, J. Comiti, and F. Fayolle, "Diffusion Coefficients of Ferricyanide Ions in Polymeric Solutions—Comparison of Different Experimental Methods," *Electrochim. Acta*, **15**, 1791(2000).
- Leuliet, J. C., J. F. Maingonnat, and G. Corrieu, "Étude de la Perte de Charge dans un Echangeur de Chaleur à Surface Raclée Traitant des Produits Newtoniens et Non-Newtoniens," *J. Food Eng.*, **5**, 153 (1986).
- Ling, S. C., "Heat Transfer from a Small Isothermal Spanwise Strip on an Insulated Boundary," *J. Heat Transfer, Trans. ASME*, 230 (1963).
- Maingonnat, J. F., J. C. Leuliet, and T. Benezech, "Modélisation de la Vitesse de Cisaillement Apparente dans un Echangeur de Chaleur à Surface Raclée. Application aux Performances Thermiques avec des Produits Non-Newtoniens," *Rev. Gén. Therm.*, **306-607**, 381 (1987).
- Mao, Z., and J. Hanratty, "Analysis of Wall Shear Stress Probes in Large Amplitude Unsteady Flows," *Int. J. Heat Mass Transfer*, **34**, 281 (1991).
- Mao, Z., and J. Hanratty, "Measurement of Wall Shear Rates in Large Amplitude Unsteady Reversing Flows," *Exp. Fluids*, **12**, 342 (1992).
- Martemianov, S. A., and A. N. Sviridov, "Mass Transfer in a Pulsating Shear Flow of Electrolyte Lacking a Directional Mean Flow," *Elektrokhimiya*, **25**, 1514 (1989).
- Naimi, M., "Étude des Lois d'Écoulement et de Transfert de Chaleur pour des Fluides Non Newtoniens en Espace Annulaire Tournant. Approche Réaliste de l'Echangeur de Chaleur à Surface Raclée", PhD Thesis ENSEM - LEMTA. INP Lorraine, France (1989).
- Nakoryakov, V. E., A. P. Burdukov, O. N. Kashinsky, and P. I. Geshv, *Electrodiffusion Method of Investigation into Local Structure of Turbulent Flows*, V. G. Gasenko Editions, Novosibirsk, Russia (1986).
- Reiss, L. P., and T. J. Hanratty, "An Experimental Study of the Unsteady Nature of the Viscous Sublayer," *AIChE J.*, **8**, 154 (1963).
- Sobolík, V., B. Benabes, and G. Cognet, "Study of Taylor-Couette Flow Using a Three-Segment Electrodiffusion Probe," *J. Appl. Electrochem.*, **25**, 441 (1995).
- Sobolík, V., J. Tihon, O. Wein, and K. Wichterle, "Calibration of Electrodiffusion Friction Probes Using a Voltage-Step Transient," *J. App. Electrochem.*, **28**, 329 (1998).
- Sobolík, V., O. Wein, and J. Cermak, "Simultaneous Measurement of Film Thickness and Wall Shear Stress in Wavy Flow of Non-Newtonian Liquids," *Collect. Czech. Chem. Commun.*, **52**, 913 (1987).
- Tihon, J., and V. Sobolík, "Dynamics of Electrodiffusion Friction Probes in Wavy Film Flow," *Proc. Int. Workshop Electrodiffusion Diagnostics of Flows*, Dourdan, France, p. 397 (1993).
- Tihon, J., J. Legrand, H. Aouabed, and P. Legentilhomme, "Dynamics of Electrodiffusion Friction Probes in Developing Annular Flows," *Exp. Fluids*, **20**, 131 (1995).
- Trommelen, A. M., and W.J. Beek, "Flow Phenomena in a Scraped Surface Heat Exchanger," *Chem. Eng. Sci.*, **26**, 1933 (1971a).
- Trommelen, A. M., and W. J. Beek, "A Mechanism for Heat Transfer in a Votator-Type Scraped-Surface Heat Exchanger," *Chem. Eng. Sci.*, **26**, 1977 (1971b).
- Tsochatzidis, N. A., and A. J. Karabelas, "Study of Pulsing Flow in a Trickle Bed Using the Electrodiffusion Technique," *J. App. Electrochem.*, **24**, 670 (1994).
- Wronski, S., and M. Jastrzebski, "Experimental Investigations of the Stability Limit of the Helical Flow of Pseudoplastic Liquids," *Rheol. Acta*, **29**, 453 (1990).

Manuscript received July 27, 1999, and revision received Dec. 17, 1999.